

# PETRIC—A Positron Emission Tomography Readout Integrated Circuit

M. Pedrali-Noy, *Member, IEEE*, G. Gruber, B. Krieger, *Member, IEEE*, E. Mandelli, *Member, IEEE*, G. Meddeler, *Member, IEEE*, W. Moses, *Senior Member, IEEE*, and V. Rosso

**Abstract**—We present the architecture, critical design issues, and performance measurements of PETRIC, a 64-channel mixed signal front-end integrated circuit for reading out a photodiode array coupled with  $\text{Lu}_2\text{SiO}_5[\text{Ce}]$  scintillator crystals for a medical imaging application: positron emission topography. Each channel consists of a low-noise charge-sensitive preamplifier, an RC-CR pulse shaper and a winner-take-all multiplexer that selects the channel with the largest input signal. Triggered by an external timing signal, a switch opens and a capacitor stores the peak voltage of the winner channel. The shaper peaking time is adjustable by means of external current inputs over a continuous range of 0.7  $\mu\text{s}$  to 9  $\mu\text{s}$ . Power consumption is 5.4 mW per channel, measured equivalent noise charge at 1- $\mu\text{s}$  peaking time, zero leakage current is 33 rms electrons plus 7.3 rms electrons per pF of input capacitance. Design is fabricated in 0.5- $\mu\text{m}$  3.3-V complementary metal-oxide semiconductor technology.

**Index Terms**—Front-end electronics, integrated circuit design, low noise, mixed signal, preamplifier, pulse shaper, winner-take-all.

## I. INTRODUCTION

WE ARE designing a positron emission tomography (PET) detector module to identify 511-keV photons generated by positron annihilation with good spatial and temporal resolution. The detector module consists of a  $8 \times 8$  cerium-doped lutetium oxyorthosilicate ( $\text{Lu}_2\text{SiO}_5[\text{Ce}]$  or LSO) scintillator crystal array coupled on one side to an  $8 \times 8$  photodiode (PD) array of 3-mm<sup>2</sup> pixels on the other to a single channel photomultiplier tube (PMT). Whenever a gamma ray interacts in the scintillator array, a timing and an energy signal are generated by the PMT and an energy signal is generated in the PD array. The PMT provides an accurate timing pulse and initial energy discrimination for the 64 crystals in the module while the PD array identifies the crystal of interaction. The sum of the charges collected at the PMT end and at the PD end, PD+PMT, provides a total energy signal while the depth estimator ratio PD/(PD+PMT) determines the depth

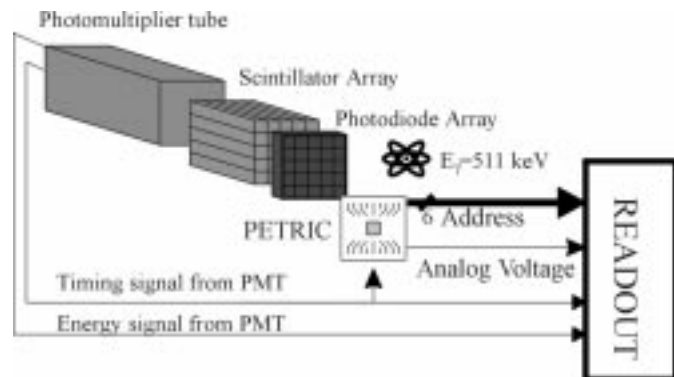


Fig. 1. Elements of the PET camera detector module. IC sits on a printed circuit board used to fan-in the PD array. IC continuously amplifies the energy signals from the PD array and produces at its output an analog pulse whose peak amplitude is proportional to the charge collected in the channel with the largest input signal (winner channel) and the 6-bit digital address of the winner channel. Timing signal from the PMT can be used to track-and-hold the output analog pulse.

of interaction (DOI) in the crystal. Fig. 1 shows the detector module.

The large number of photons generated by the LSO crystal during 511-keV gamma interaction (3000 to 5000) makes the noise due to statistical fluctuation in photon emission in the PMT negligible. The electronic noise at the PD end is important, given the constraints of the detector capacitance ( $\sim 3$  pF), detector leakage current (300 pA) and rate (peaking time  $\sim 1$   $\mu\text{s}$ ) and, thus, must be minimized [1]. The identification of the crystal of interaction has to occur in a short time compared to the expected period between different input events (10- $\mu\text{s}$ /detector module).

PETRIC provides a unique mixed-signal solution to readout the signals from PD array through the novel on-chip integration of an array of highly sensitive amplifier channels with a winner-take-all (WTA) multiplexer.

## II. INTEGRATED CIRCUIT REQUIREMENTS AND IMPLEMENTATION

The use of complementary metal-oxide-semiconductor (CMOS) amplifiers for PET front-end electronics using p-i-n diode arrays was evaluated in [2]. Our integrated circuit (IC) has to simultaneously acquire input signals and perform analog and digital readout; it can be set in the desired configuration (gain, channel masking) before acquisition and readout begin. Input signals come from a 64 pixel PD array direct current (dc)

Manuscript received November 5, 2000; revised March 8, 2001. This work was supported in part by the U.S. Department of Energy under Contract DE-AC03-76SF00098 and in part by the Public Health Service under Grants P01-HL25840 and R01-CA67911.

M. Pedrali-Noy was with the Lawrence Berkeley National Laboratory, Integrated System Group, Berkeley, CA 94709 USA. He is now with Qualcomm, San Diego, CA 92121 USA (e-mail: marziop@qualcomm.com).

G. Gruber, B. Krieger, E. Mandelli, G. Meddeler, and W. Moses are with the Lawrence Berkeley National Laboratory, Berkeley, CA 94709 USA.

V. Rosso is with the Dipartimento di Fisica dell'Universita' e sezione INFN, San Piero a Grado, Pisa 56010, Italy.

Publisher Item Identifier S 0018-9499(01)05079-1.

coupled to the IC; each PD has a shunt capacitance  $C_d$  of  $\sim 3$  pF and a dark leakage current  $I_{\text{dark}}$  in the range of 100–600 pA. The IC continuously outputs the amplified pulse signal corresponding to the element of the array with the highest signal and its digital address. The peaking time and the gain must be adjustable to comply with different signal/data-rate systems. An externally generated track-and-hold signal stores the pulse peak voltage on an on-chip capacitor. Electronic noise should dominate; therefore it must be minimized. To achieve a reasonable signal-to-noise ratio, the total input referred noise should be less than 200 electrons rms. Noise contributions from the electronic readout and from the leakage current of the detector have been studied extensively in the field of electronics for high-energy physics experiments [3]. Power consumption should be minimized since the module that hosts the IC does not provide cooling. We have selected a  $0.5\text{-}\mu\text{m}$  3.3-V CMOS technology with silicide block and linear capacitor options based on current availability. We have fabricated and tested a 16-channel amplifier prototype and a 16-channel WTA prototype; these prototype designs, with minimal modification, were merged and expanded to realize the 64-channel IC. Noise coefficients for  $1/f$  noise extracted from prototype measurement showed that the  $1/f$  noise contribution to the equivalent noise charge (ENC) is relevant at our target peaking time and input leakage current.

The chip architecture is shown in Fig. 2. Input charge signals are pre-amplified and filtered to optimize signal to noise ratio. The WTA circuit, dc coupled to the amplifier outputs, continuously selects the channel with the largest input and connects it to an output buffer.

A dummy channel, without an amplifier, presents a dc-only voltage to the WTA and acts like a threshold that the other channels need to exceed in order to be identified as the winner. The dummy channel should be selected when no input signal comes from the PD array and prevents the WTA from switching due to electronic noise. The choice of the threshold voltage comes from consideration of several factors: the random electronic noise at the output of the amplifier channel, the noise coupling from the switching circuit to the sensitive amplifiers, the dc output dispersion of the amplifiers, and the dc input dispersion of the WTA. The threshold should be large enough to prevent switching due to noise, while it should be small enough to allow identification of small signals.

Triggered by an off-chip signal, a track-and-hold capacitor can store the analog peak voltage. The control logic sets the preamplifiers' gains, masks individual channels from the WTA, and connects a calibration circuit for testing. For minimum crosstalk between the digital and the sensitive analog sections, it is possible to gate the digital signal from the WTA to the encoder; in this way, the encoder can be activated after the peak voltage has been stored in the holding capacitor.

### III. CIRCUIT DESIGN AND LAYOUT

#### A. Amplifier Channel

The amplifier channel consists of a low-noise charge-sensitive amplifier (CSA) followed by an  $RC$ - $CR$  shaper and an alternating current (ac) amplifier.

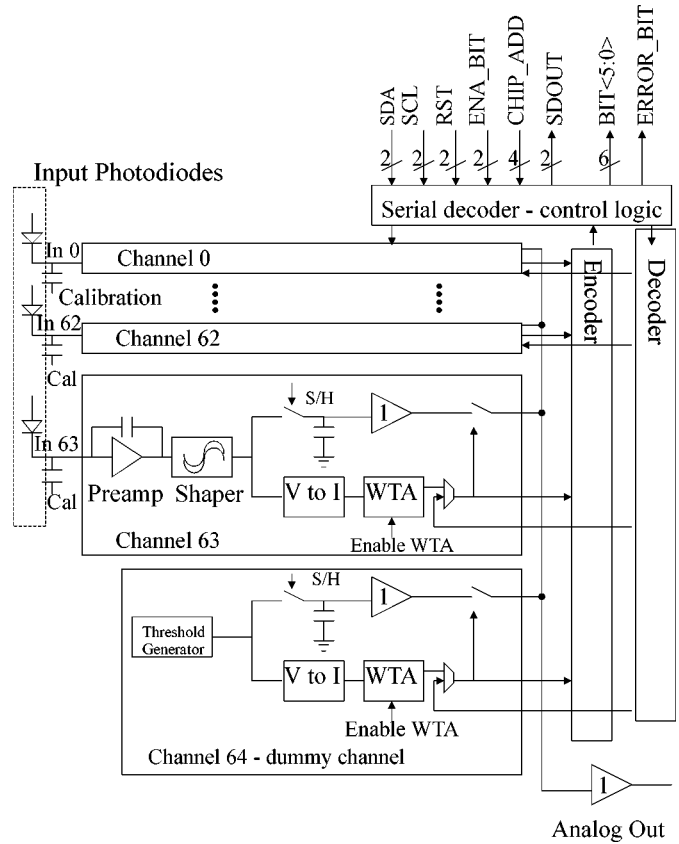


Fig. 2. PETRIC architecture. Each channel consists of a pulse amplifier (CSA and  $RC$ - $CR$  filter) and a WTA cell. When a WTA cell recognizes its amplifier channel as producing the largest output voltage, a hit bit is generated. This bit is encoded to produce the address of the winner channel.

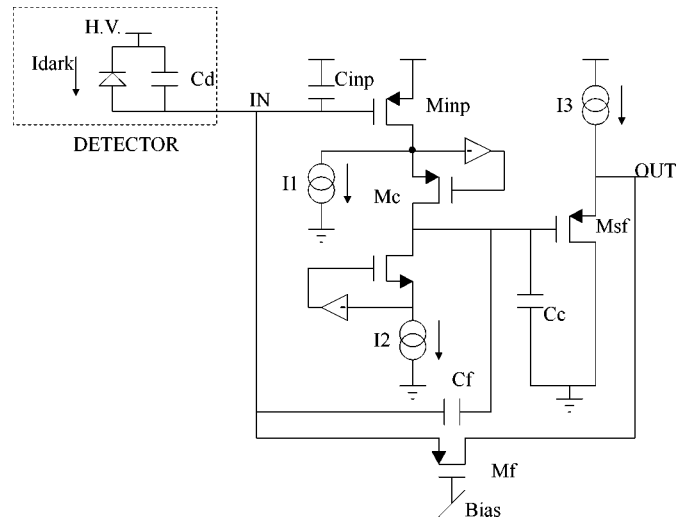


Fig. 3. Simplified schematic of the CSA. Telescopic cascode design still fits in 3-V power supply, but will require folding for lower voltage operation.

1) *Charge-Sensitive Preamplifier:* The single-ended CSA consists of a common source cascode stage with regulated cascodes to boost dc gain followed by a source follower stage. A simplified schematic is shown in Fig. 3. The input device  $M_{\text{inp}}$  is a p-channel MOS (PMOS) with gate capacitance  $C_{\text{inp}}$ ; the size of  $M_{\text{inp}}$  has been chosen as a compromise between  $1/f$  noise minimization for a MOS in strong inversion ( $C_{\text{inp}} = C_d$ )

and thermal noise minimization ( $C_{\text{imp}} = 1/3C_d$ ) [4]. The bias current of  $M_{\text{imp}}$ , given by  $I_{\text{imp}} = I_1 + I_2 \sim 900 \mu\text{A}$ , sets  $M_{\text{imp}}$  in the region of operation at the onset of strong inversion to obtain a reasonable  $g_m/I_{\text{imp}}$  ratio while achieving a high transconductance  $g_m \sim 8 \text{ mS}$  [5]. The main noise contribution to the noise of the CSA comes from  $M_{\text{imp}}$ , although the noise contribution from the current sources  $I_1$  and  $I_2$  are not negligible due to the low power supply and the limited voltage available to degenerate them [6]. The feedback capacitance  $C_f$  is placed between the input node IN and the gate of the source follower stage to avoid introduction on the closed loop of the complex poles of the follower stage and to isolate the feedback capacitor from the following stage. Switching between different feedback capacitors allows different gains to be achieved. The low-level input signal requires a small feedback capacitance to achieve a reasonable gain at the preamplifier output. With a choice of  $C_f = 14 \text{ fF}$  for the maximum gain setting in the preamplifier, the feedback factor  $f$ , given by

$$f = \frac{C_f}{C_d + C_{\text{imp}} + C_{\text{parasitic}}} \quad (1)$$

is  $f = 2.3 \times 10^{-3}$ . This small feedback factor provides high gain and relaxes the design constraints for closed loop stability at the expense of a slower response of the preamplifier due to the small value of  $f$  the regulated cascodes are essential for achieving sufficient close loop gain. Charge restoring is provided by minimum length PMOS reset transistor  $M_f$  ( $W/L = 2.4/0.6 \mu\text{m}$ ).  $M_f$  is biased to operate in the saturation in quiescent conditions and it enters in strong inversion when a charge signal is detected.  $M_f$  adds negligible parasitic capacitance to the feedback capacitance, although its minimum size could result in a spread of its output resistance due to transistor mismatch and, thus, affect the preamplifier performance inducing channel-to-channel reset time variations. Achieved drain-to-source resistance  $R_{ds}$  is  $14\text{--}3 \text{ G}\Omega$  in the  $100\text{--}500 \text{ pA}$  range; at zero leakage current, the maximum achievable  $R_{ds}$  is limited by the MOS source and drain diode leakage current to  $70 \text{ G}\Omega$ . The dc biasing of  $M_f$  is provided by a replica bias like in [7]; differently from [7], no pole/zero compensation is provided. Due to the direction of the leakage current,  $M_f$  operates at constant gate-to-source voltage; a large spread in the leakage current dictates adjustment of the bias on a channel-by-channel basis. This is accomplished by an on-chip digital/analog converter.

2) *Pulse Shaper*: The pulse shaper is a two stage Gm-C filter and it is a single-ended first-order version of the design presented in [8]. A simplified schematic is shown in Fig. 4. The two identical operational transconductance amplifiers (OTAs) OTA1 and OTA2 that determine the time constants are based on the design presented in [9]; they use transistors operated in the triode region to degenerate their input differential pairs. The OTAs' tail current can be externally adjusted to modify their transconductance and achieve the desired peaking time. The filter is followed by an ac amplifier that provides no shaping, due to the long time constant introduced by OTA3 and its feedback capacitance; this block eases the requirements of large signal linearity of the preceding blocks at the expense of power consumption. It should be noted that an ac coupling along the amplifying chain generates a shift of the output baseline at high data rates, as described in [10].

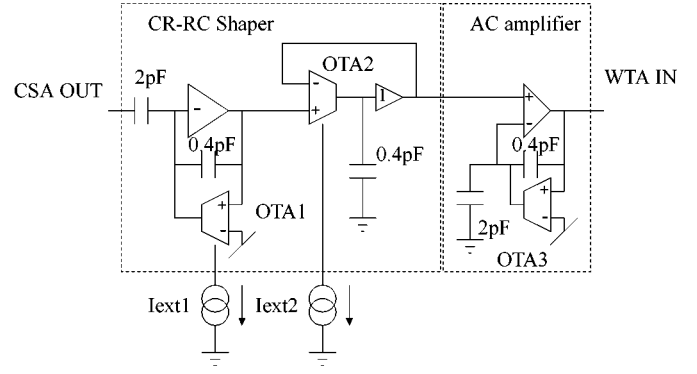


Fig. 4. Simplified schematic of the pulse shaper. Two external currents  $I_{\text{EXT}1}$  and  $I_{\text{EXT}2}$  are used to tune the transconductances of the OTAs and, thus, to change the pulse peaking time.

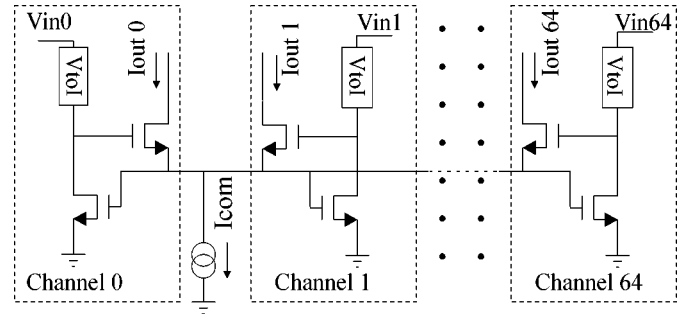


Fig. 5. Simplified schematic of the WTA. Based on a two-transistor per cell design, this circuit is compact and dissipates very little power.  $I_{\text{COM}}$  is set equal to  $15 \mu\text{A}$  by an external reference.

## B. WTA

The WTA circuit is dc coupled to the previous amplifier stage and is based on the design presented in [11]; it consists of a voltage-to-current ( $V$ to $I$ ) converter followed by a high gain nonlinear differential circuit. A simplified schematic is shown in Fig. 5. The  $V$ to $I$  circuit consists of a resistor followed by a common gate stage. The WTA cells in each channel share a common tail current  $I_{\text{COM}}$  that is taken by the channel with the largest input, like in a large-signal driven differential pair. The channel with the highest input voltage has  $I_{\text{OUT}} = I_{\text{COM}}$  while all the others  $I_{\text{OUT}}$  is  $\sim 0$ ; a current comparator compares the output current of each channel to a fixed current and generates the logic signal that identifies the winning channel. Due to its high gain, the main source of error of the WTA comes from mismatch of the transistors and resistors in the  $V$ to $I$ . The selection circuit is designed to have a first-order response and a gain-bandwidth product of  $8 \text{ MHz}$ .

A dc level shifter sets the dc output voltage of the dummy channel  $\sim 40 \text{ mV}$  above the other channels.

When a switch is toggled by an external signal, the track and hold capacitor stores the analog voltage from the preceding stage; charge injection and clock feedthrough are minimized by a compensation scheme [12].

## C. Control Logic

The digital control section has been synthesized from a state-machine diagram using standard cells. The logic uses static fully synchronous CMOS registers. Decoding a digital protocol based

on the Xicor I2C, this logic circuit controls the gain and reset time constant of the preamplifiers, masks out unwanted channels from the WTA, connects different channels to the calibration capacitance, and produces an error bit when multiple channels are selected. The IC can be set to operate in two different modes: in WTA (default) mode the WTA selects the channel with the highest output signal. In MUX (test) mode, the WTA is disabled and a channel selected by the user is connected to the analog output.

#### D. Layout

Fig. 6 shows a microphotograph of the realized circuit. To minimize coupling to the sensitive amplifier from the switching circuitry, separate quiet power supply lines and pads have been utilized for the input transistors' supply, the input transistors' well, and the amplifier channel; the WTA, the encoder, and the digital section share the same supplies. Nonpower carrying substrate contact lines are employed. Furthermore, to take advantage of the low resistive substrate and to reduce substrate noise coupling, the chip back has been gold plated [13]. The layout is pad-limited: the bond pad size and spacing have been dictated by minimum line pitch and bonding constraints on the fan-in printed circuit board that will host the IC. The die area is 4.5 mm  $\times$  4.8 mm. The capacitors in the preamplifiers are realized as Metal 1 to Metal 2 plates while all the other capacitors are implemented using the linear capacitor option, i.e., polysilicon-thin\_oxide-n+diffusion. Test pads have been provided at the output of the CSAs, shapers, and ac amplifiers and to monitor the status of the internal digital logic.

### IV. PERFORMANCE MEASUREMENTS

#### A. Amplifier Channel

1) *Gain*: We measured the gain of the amplifier's channel using external injection capacitors. Fig. 7 shows the waveforms present at the analog output when different charges are injected into one amplifier. At maximum gain setting (120 mV/1000 e<sup>-</sup>), 1- $\mu$ s peaking time (achieved with equal RC and CR time constants in the shaper), detector capacitance  $C_d = 3.7$  pF, the gain is linear within 1% in the range of 750 to 4000 electrons input charge. For higher input charges (5 ke<sup>-</sup> to 9 ke<sup>-</sup>), the nonlinearity of the pulse shaper degrades the performance and finally the output stage enters into saturation for input charges bigger than 9 ke<sup>-</sup>.

Using the internal calibration circuit, we have measured 3% relative rms gain dispersion between channels on the same IC.

2) *Pulse Shaping*: Adjusting the external currents peaking times are achievable in the range of 0.7–9  $\mu$ s as shown in Fig. 8.

3) *DC Output Offset Voltage*: The dc dispersion at the output of the amplifier channel is determined by the input random offset of the feedback transconductor of the ac amplifier. Measurements show a value for the dc offset variation of 8-mV rms.

4) *Electronic Noise*: Noise measurements were performed on a test board since a detector module was not yet available at the time of publication of this paper. The characterization of the chip noise performances was carried out on both unbonded channels (no external load) and on channels that were bonded

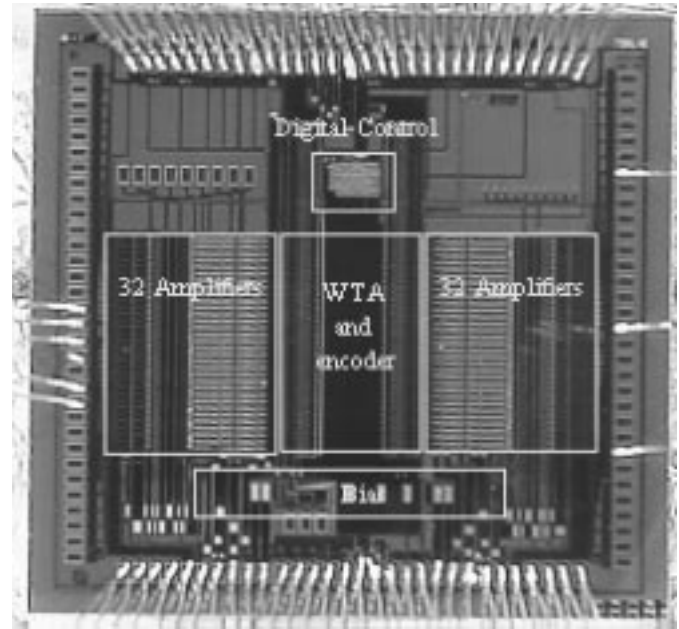


Fig. 6. Microphotograph of the realized IC. 64 channels are split in two columns and they share a common bias; the WTA cells sit in the center, the digital control logic is on top.

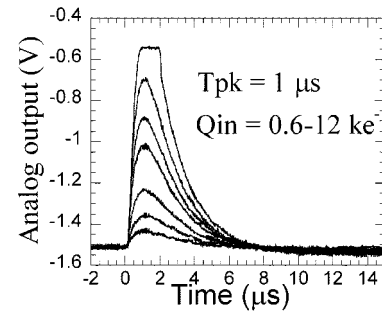


Fig. 7. Voltage output response of a single amplifier channel to different input charges.

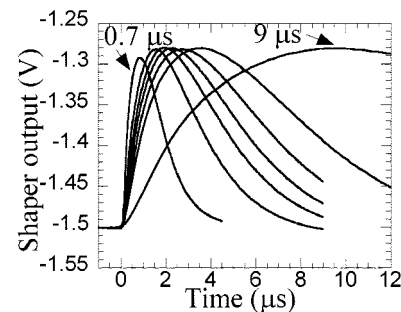
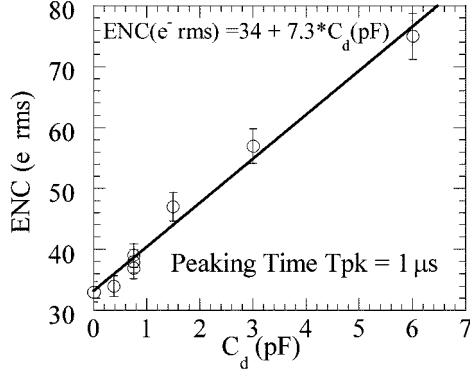


Fig. 8. Voltage output response of a single channel to an 1800 electrons input charge for different values of the external current sources of the shaper stage.

to outside loading capacitors. Input ENC was measured on each channel as the standard deviation of the output peak voltage distribution, assumed to be Gaussian. In Fig. 9, the results of the measurements are plotted as a function of the input external capacitance at a filter peaking time setting of 1  $\mu$ s. Even if these data do not take into account any leakage detector current, the results confirm noise performances well below the required 200 electrons specification for a foreseen 3-pF load. Noise performances were also measured as a function of the filter peaking


 Fig. 9. ENC versus detector capacitance  $C_d$  at  $1 \mu\text{s}$  peaking time.

time setting as plotted in Fig. 10 to extrapolate the  $1/f$  noise floor limit for three different input capacitances. The data in this plot report a dominance of white noise contribution until  $10\text{-}\mu\text{s}$  peaking time and confirm an ENC scaling with capacitance equal to  $7.2$  electrons per pF. As a crosscheck, input referred noise spectral density was extracted from measurements and compared to the expected one. In a linear system, the input referred noise charge can be expressed as

$$\text{ENC}^2 = S_W \frac{A_1}{\tau} C_{\text{TOT}}^2 + A_2 C_{\text{TOT}}^2 S_{1/f} + A_3 \tau S_{//} \quad (2)$$

where

- $S_W$  input noise spectral density;
- $S_{1/f}$  flicker noise spectral density;
- $S_{//}$  parallel noise spectral density;
- $A_1$  white series noise coefficient;
- $A_2$   $1/f$  series noise coefficient;
- $A_3$  parallel noise coefficient;
- $C_{\text{TOT}}$  total input capacitance;
- $\tau$  filter peaking time [14].

At  $1\text{-}\mu\text{s}$  peaking time, the filter bandwidth is large enough to assume that the white noise contribution to the total input noise is dominant, in absence of parallel noise. The relation between ENC and input capacitance is linear and the input white noise spectrum can be inferred from the measurements

$$S_w = \frac{\tau}{A_1} \left[ \frac{\partial \text{ENC}}{\partial C_D} \right]^2. \quad (3)$$

Acquiring with a digital oscilloscope the voltage waveform at the output of the shaper we measured the values of the noise coefficients  $A_1$ ,  $A_2$ , and  $A_3$ . With a measured  $A_1$  value close to one, the preamplifier input white noise spectral density is  $1.3 \text{ nV}/\sqrt{\text{Hz}}$  in agreement with the simulation results. Data in Fig. 10 confirm the result with and extracted  $1.4 \text{ nV}/\sqrt{\text{Hz}}$  against an input device simulated noise of  $1.2 \text{ nV}/\sqrt{\text{Hz}}$ .

### B. Amplifiers and WTA

**1) Channel Selection:** The WTA selects the input channel with the highest dc voltage in less than  $150 \text{ ns}$ , connects it to the analog buffer amplifier, and outputs the digital address bits of the winning channel. In Fig. 11 two recognizable  $RC\text{-}CR$  shaped pulse are shown at the analog output of the IC. The time that the WTA takes to identify the winner channel is the sum of the switching times of the WTA cell, the current comparator, and the decoder.

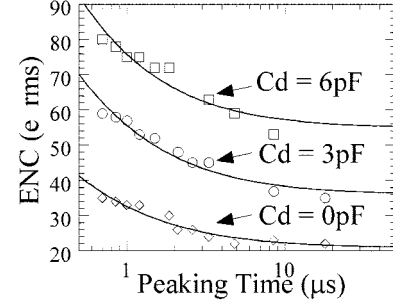


Fig. 10. ENC versus peaking time for different detector capacitances. Data are fitted neglecting the parallel noise contribution.

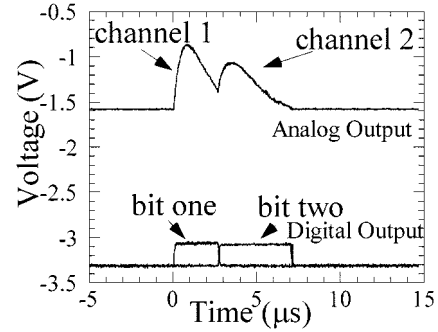
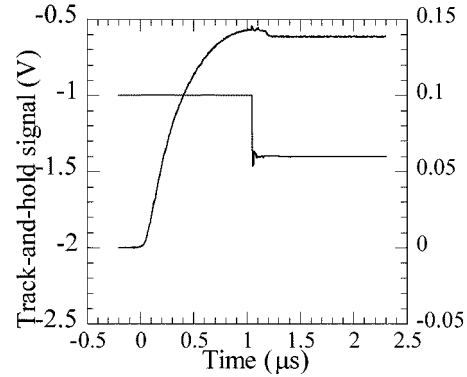

 Fig. 11. Two different input signal charges are injected in two different channels. The first signal  $Q_1$  is injected at time zero while the second signal  $Q_2$  ( $Q_1 > Q_2$ ) is injected after  $\sim 2.5 \mu\text{s}$ . Analog output tracks the pulse generated by  $Q_1$  until the pulse generated by  $Q_2$  becomes higher in voltage. Digital output bits toggle accordingly.


Fig. 12. Analog voltage is stored in the holding capacitor when the track-and-hold signal toggles.

**2) Input DC Threshold Dispersion:** Connecting two channels at the time to the WTA, one channel with no input signal and the dummy threshold channel, we have varied the threshold channel voltage until the other channel would be identified as the winner. We have measured  $20\text{-mV}$  rms dc dispersion at the input of the WTA. This value is the sum of the output dispersion of the amplifier channel and of the input dispersion of the WTA channel. Since the measured dc output dispersion of the amplifiers is  $8\text{-mV}$  rms, it is the WTA circuit input dispersion that dominates. When no input signal is present at the amplifier inputs, the dummy channel is always selected as the winner by the WTA.

**3) Track-and-Hold:** The output analog voltage of the amplifier channel is stored in a  $400\text{-fF}$  holding capacitor when the hold signal is received by the IC. Track-and-hold operation is shown in Fig. 12. The measured voltage error in the holding ca-

TABLE I  
SUMMARY OF THE IC'S PERFORMANCES

| Technology                   | CMOS 0.5 $\mu\text{m}$ 3.3 V       |
|------------------------------|------------------------------------|
| Die Area                     | 4.5 mm x 4.8 mm                    |
| Leakage Current              | 30 – 600 pA                        |
| Detector Capacitance         | 3 pF                               |
| Number of Channels           | 64                                 |
| Max Gain                     | 120mV/1000e <sup>-</sup>           |
| Min Gain                     | 40 mV/1000e <sup>-</sup>           |
| Shaping                      | 0.7 to 9 $\mu\text{s}$ unipolar    |
| Noise at 1 $\mu\text{s}$ Tpk | 34 + 7.2*Cd(pF) e <sup>-</sup> rms |
| Power                        | 5.4 mW/Channel                     |

pacitor due to clock feedthrough and charge injection is less than 4 mV; the error is signal dependent and could be minimized increasing the holding capacitor size from its current value at the expense of loading the previous stage.

The performances of the IC are summarized in Table I.

### V. CONCLUSION

Compactness, high performances, and flexibility make PETRIC a unique and ideal solution for PET camera modules front-end readout utilizing p-i-n diode arrays for position and DOI detection. Due to the flexibility of its architecture and of the analog front end, the IC is well suited for any application employing low capacitance PD detectors in moderate to high data rate environments and it is currently considered for single photon cameras readout [15].

Future directions of this work include on-chip integration of a peak detection circuit and band-gap voltage reference, a self-adjusting reset scheme in the preamplifier and a characterization of the electrostatic discharge protection structures for production development.

### ACKNOWLEDGMENT

The authors would like to thank Prof. P. F. Manfredi for the fruitful discussions, M. Ho for designing the test boards and the detector module, and G. Zizka for bonding several ICs.

### REFERENCES

- [1] J. Huber, W. Moses, M. Andreaco, and O. Petterson, "An LSO scintillator array for a PET detector module with depth of interaction measurement," *IEEE Trans. Nucl. Sci.*, pp. 684–688, June, 2001.
- [2] W. Moses, I. Kipnis, and M. Ho, "A 16-channel charge sensitive amplifier IC for a PIN PD array based PET detector module," *IEEE Trans. Nucl. Sci.*, vol. 41, pp. 1469–1472, Aug. 1994.
- [3] E. Gatti and P. Manfredi, "Processing the signals form solid-state detectors in elementary particle physics," *Nuovo Cimento*, vol. 9, no. I, pp. 1–145, Apr. 1986.
- [4] Z. Chang and W. Sansen, *Low-Noise Wide-Band Amplifiers in Bipolar and CMOS Technology*. Norwell, MA: Kluwer, 1991.
- [5] K. Larker and W. Sansen, *Design of Analog Integrated Circuit and Systems*. New York: McGraw-Hill, 1994, p. 31.
- [6] P. O'Connor and G. De Geronimo, "Prospects for charge sensitive amplifiers in scaled CMOS," in *IEEE Nuclear Science Symp. Conf. Record*, vol. 1, Oct. 1999, pp. 89–93.
- [7] G. Gramegna, P. O'Connor, P. Rehak, and S. Hart, "CMOS preamplifier for low-capacitance detectors," *Nucl. Inst. Methods*, vol. A 390, pp. 241–250, May 1997.
- [8] B. Krieger, I. Kipnis, and B. Ludewigt, "XPS: A multi-channel preamplifier-shaper IC for X-ray spectroscopy," *IEEE Trans. Nucl. Sci.*, vol. 45, pp. 732–734, 1998.
- [9] F. Krummenacher and N. Joehl, "A 4-Mhz continuous-time filter with on chip automatic tuning," *IEEE J. Solid-State Circuits*, vol. 23, pp. 750–758, June 1988.
- [10] E. Gatti and P. Manfredi, "Processing the signals form solid-state detectors in elementary particle physics," *Nuovo Cimento*, vol. 9, no. I, p. 123, Apr. 1986.
- [11] W. Moses, E. Beuville, and M. Ho, "A winner-take-all IC for determining the crystal of interaction in PET detectors," *IEEE Trans. Nucl. Sci.*, vol. 43, pp. 1615–1618, June 1996.
- [12] J. Shieh, M. Patil, and B. Sheu, "Measurement and analysis of charge injection in MOS analog switches," *IEEE J. Solid-State Circuits*, vol. SSC-22, pp. 277–281, Apr. 1987.
- [13] D. Su, M. Loinaz, S. Masui, and B. Wooley, "Experimental results and modeling techniques for substrate noise in mixed-signal ICs," *IEEE J. Solid-State Circuits*, vol. 28, p. 426, Apr. 1993.
- [14] V. Radeka, "Signal, noise and resolution in position-sensitive detectors," *IEEE Trans. Nucl. Sci.*, vol. 21, p. 51, Feb. 1974.
- [15] G. Gruber, W. Choong, W. Moses, S. Derenzo, S. Holland, and M. Pedrali-Noy *et al.*, "Performance of a compact 64-pixel CsI(Tl)/Si PIN PD imaging module with IC readout," *IEEE Trans. Nucl. Sci.*, submitted for publication.